Evolutionary constraints on visual cortex architecture from the dynamics of hallucinations

Thomas Charles Butler[a,b], Marc Benayoun[c], Edward Wallace[d,e], Wim van Drongelen[c], Nigel Goldenfeld[a,1], and Jack Cowan[e]

[a]Department of Physics, University of Illinois, Urbana-Champaign, 1110 West Green Street, Urbana, IL 61801; [b]Department of Physics, Massachusetts Institute of Technology, 77 Massachusetts Avenue, Cambridge, MA 02139; [c]Department of Pediatrics, University of Chicago, Chicago, IL 60637; [d]Faculty of Arts and Sciences Center for Systems Biology, Harvard University, Cambridge, MA 02138; and [e]Department of Mathematics, University of Chicago, Chicago, IL 60637

Contributed by Nigel Goldenfeld, November 22, 2011 (sent for review April 12, 2011)

In the cat or primate primary visual cortex (V1), normal vision corresponds to a state where neural excitation patterns are driven by external visual stimuli. A spectacular failure mode of V1 occurs when such patterns are overwhelmed by spontaneously generated spatially self-organized patterns of neural excitation. These are experienced as geometric visual hallucinations. The problem of identifying the mechanisms by which V1 avoids this failure is made acute by recent advances in the statistical mechanics of pattern formation, which suggest that the hallucinatory state should be very robust. Here, we report how incorporating physiologically realistic long-range connections between inhibitory neurons changes the behavior of a model of V1. We find that the sparsity of long-range inhibition in V1 plays a previously unrecognized but key functional role in preserving the normal vision state. Surprisingly, it also contributes to the observed regularity of geometric visual hallucinations. Our results provide an explanation for the observed sparsity of long-range inhibition in V1—this generic architectural feature is an evolutionary adaptation that tunes V1 to the normal vision state. In addition, it has been shown that exactly the same long-range connections play a key role in the development of orientation preference maps. Thus V1's most striking long-range features—patchy excitatory connections and sparse inhibitory connections—are strongly constrained by two requirements: the need for the visual state to be robust and the developmental requirements of the orientational preference map.

evolution | fluctuations

The primary visual cortex, V1, represents external stimuli as patterns of neural excitation. In the normal state, patterns of excitation on V1 are driven by sensory stimuli generated in the retina mapped to V1 from the visual field by the retinocortical map (1, 2). Patterns seen as visual hallucinations arise in exceptional circumstances when external stimuli are overwhelmed by internally generated spontaneous patterns of neural excitation. This situation occurs when the circuit parameters governing the dynamics of V1 are changed, for example, through the influence of psychotropic drugs that may act in part through effectively weakening cortical inhibition (3). The mechanism governing spontaneous pattern formation has been shown in previous studies to be closely related to that of diffusion driven pattern formation in chemical and other biological systems, known as the Turing mechanism (4–6). Compelling evidence for this mechanism has been provided by previous studies that have shown that precisely the four basic classes of geometric visual hallucinations (or form constants) and no others, commonly reported by subjects (7), follow directly from the Turing mechanism and spontaneous symmetry breaking of the basic approximate symmetries of V1 associated with translation and orientation preference (6). Here we show that V1 is specially configured to *avoid* the formation of visual hallucinations and remain stable under typical operating conditions in the visual state. Together with recent reports of developmental plasticity in V1 (8), and the apparent universality of the self-organizing principles behind the structure of its orientation columns (9), our results imply strong constraints on the key features and evolution of its global architecture at intermediate length scales.

We analyze and compare two classes of model for the spatiotemporal dynamics of neural excitation in V1. The first model is subject to network connections that are similar to the real V1 network, whereas the second model represents a family of a priori physiologically plausible alternative network structures. We show that the alternative network structures substantially degrade normal visual function, thereby illuminating the functional advantages of the network structure actually realized in V1. Similar approaches have been successfully applied to other robust phenomena in biology, such as embryonic pattern formation (10), bistable genetic switching (11), and the generation of temporal oscillations of gene expression (12). In these cases, the requirement that the network dynamics robustly preserve some function under variation of parameters or noise led naturally to the elucidation of key features such as the coupling of positive and negative feedback loops to generate robust oscillations in the level of gene expression (12). We will show that the requirement that V1 activation be primarily driven by external sensory stimuli strongly constrains the topology of its connections by allowing only sparse long-range inhibition. This feature of V1 is well-established empirically (13), but has not yet been explained. In other parts of the cortex where the function is presumably different, there is some evidence that sparse long-range connections do exist that provide some lateral disinhibition (14, 15). By combining this requirement with the recent experimental confirmation of calculations that predict that long-range interactions between V1 neurons are essential for stabilizing the development of orientational preference maps (9), we obtain sufficient constraints on V1 network structure to strongly constrain the character of its long-range connections.

Geometric visual hallucinations arise through a variant of the Turing mechanism for pattern formation (4). In V1, spatial patterns arise when the range of local excitatory to inhibitory connections (E–I) is sufficiently longer than the range of excitatory to excitatory (E–E) connections. Thus when there is a local burst of excitation, the longer-ranged connections to inhibitory neurons contain the burst. Fluctuations of activity are then confined over some characteristic length scale, leading to spatial pattern formation. The difference in length scale of E–E connections versus E–I connections results in an effective "Mexican hat" potential if inhibitory neurons are integrated out, exactly as required for

Author contributions: T.C.B., N.G., and J.C. designed research; T.C.B., M.B., E.W., W.v.D., N.G., and J.C. performed research; and T.C.B., E.W., N.G., and J.C. wrote the paper.

The authors declare no conflict of interest.

[1]To whom correspondence should be addressed. E-mail: nigel@illinois.edu.

This article contains supporting information online at www.pnas.org/lookup/suppl/doi:10.1073/pnas.1118672109/-/DCSupplemental.

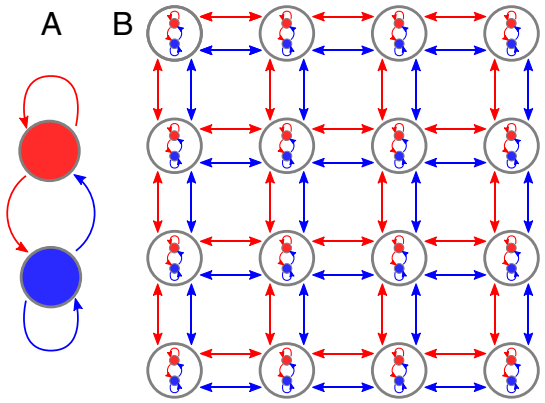

Fig. 1. (*A*) Simplified Douglas–Martin microcircuit. The blue circle corresponds to inhibitory neurons, and the red circle to excitatory neurons. Similarly, excitatory connections are shown as red arrows from their source and inhibitory connections as blue arrows. Inputs to the microcircuit vary and are not shown. (*B*) Simplified representation of patchy connections between hypercolumns in V1. Each hypercolumn is represented by a circle, with both *E–E* and *E–I* connections between hypercolumns indicated by red arrows.

the successful development of a stable orientation preference map (9).

Model

We model each local hypercolumn using the most general possible wiring, consistent with the physiological separation of excitatory and inhibitory neurons. Alternatively, the local structure can be viewed as many copies of a simplified version of the Douglas–Martin canonical microcircuit (16). This microcircuit is shown schematically in Fig. 1*A*.

We now introduce a model of V1 as a two-dimensional lattice of canonical microcircuits. To capture the lattice structure, we distinguish two length scales. The first length scale is local and is the one on which canonical microcircuits, each of which has a width of approximately 100 μm, interact with their neighbors. We model this local scale as comprising all the approximate 10 microcircuits in one V1 hypercolumn (1). Based on neuroanatomical data, our model includes excitatory and inhibitory connections between all microcircuits within a hypercolumn (17).

The second length scale is longer ranged. On this length scale, hypercolumns are coupled together by patchy excitatory connections. These connections have a range of approximately 4 mm with axonal arbors every 1 mm or so (18). Thus they are between hypercolumns. If we take the lattice spacing between individual microcircuits to be L mm, then the spacing between hypercolumns is $\sqrt{a}L$ mm where a is the number of microcircuits per hypercolumn. Thus the connections between differing lattice sites support a mixture of both local and nonlocal or lattice scale excitation and inhibition. These couplings are as shown in Fig. 1. For even longer-ranged connections, which would provide a third length scale, the best evidence to date (19) suggests that they are small world (20). However, in this paper, we do not consider their effects. The model presented here is a special case of that introduced to analyze the formation of geometric visual hallucinations (6). As we note later, it is also closely related to a model of the cortex introduced to study the development of stable orientation preference maps (9, 21).

These assumptions yield variants of the Wilson–Cowan equations (22) for local density of neural excitation of excitatory (φ) and inhibitory (ψ) neurons (see *SI Text*). On length scales much greater than the lattice scale, the Wilson–Cowan equations reduce to the partial differential equations

$$\partial_t\varphi = -\alpha_E\varphi + (1-\varphi)f_E[s_I^E] \qquad \partial_t\psi = -\alpha_I\psi + (1-\psi)f_I[s_I^I] \quad \textbf{[1]}$$

with currents given by

$$s_E = w_{EE}(1+g_{EE}^1\Delta)\varphi - w_{EI}(1+g_I^1\Delta)\psi + h_E$$
$$s_I = w_{IE}(1+g_{IE}^1\Delta)\varphi - w_{II}(1+g_I^1\Delta)\psi + h_I. \quad \textbf{[2]}$$

The functions f_I and f_E are sigmoidal and capture the saturating response of neurons to external stimuli. The symbol Δ represents the continuous Laplacian in two dimensions. The matrix W captures the local synaptic interactions as in Fig. 1*A*; for example, w_{IE} denotes the synaptic weight of *E–I* connections. The parameters g_{ij}^1 are effective length scales of the indicated connections, and we take $g_{EI} = g_{II} = g_I$. For the purposes of this study of spontaneous pattern formation, external stimuli h are set to zero. Although most of the key conclusions of the present work are analytical, typical simulation parameters are $w_{EE} = 1.3$ with all other $w = 1$, $\alpha_I = \alpha_E = 0.1$. The lattice scale spacing is taken in units of $\sqrt{g_{EE}^1}$. Previously cited neuroanatomical data (13) indicates that $g_I^1 \ll g_{IE}^1$.

Results

Provided couplings that promote excitation, such as w_{EE}, are sufficiently large compared to relaxation and inhibitory couplings, Eq. Eq. **1** with lattice scale effects neglected ($g_{ij}^1 = 0$), support a stable fixed point at nonzero excitation levels of both excitatory and inhibitory neurons. When such effects are restored, normal vision corresponds to a stable homogeneous steady state. Failure of normal vision to geometric visual hallucinations occurs when the homogeneous steady state becomes unstable to spatially inhomogeneous perturbations, leading to regular pattern formation (see Fig. 2*A*).

The exotic spiral structure of hallucinations reported by patients (7) and shown in Fig. 2*B* arises from regular pattern formation through the retinotopic map. The retinotopic map transforms coordinates of excitation on V1 into visual field coordinates through an approximate logarithmic conformal map, as demonstrated experimentally in ref. 2. When regular patterns are subjected to a logarithmic conformal map, they are transformed into logarithmic spiral patterns, implying that regular pattern formation on V1 results in the logarithmic spiral patterns observed in geometric visual hallucinations (5).

In the full model above, with $g_I^1/g_{EE}^1 \ll 1$ as physiologically motivated, geometric hallucinations occur when

$$\frac{g_I^1}{g_{EE}^1} > \frac{w_{EE}[\alpha_I + f_I + (1-\psi)f_I' w_{II}]}{w_{EI}(1-\psi)f_I' w_{IE}} + O\left(\frac{g_I^1}{g_{EE}^1}\right), \quad \textbf{[3]}$$

where all functions, derivatives, and concentrations of firing inhibitory neurons are evaluated at the homogeneous fixed point (see *SI Text*). Such conditions may possibly be achieved through the effects of hallucinogenic drugs (5, 7).

How would V1 behave if extensive lattice scale *I–I* connections were present? This extensive lattice scale inhibition means that inhibitory activity in one microcircuit suppresses inhibition in distant microcircuits, leading to more excitatory activity in the distant site: *I–I* connections tend to enhance negatively correlated fluctuations in activity. We introduce such connections by relaxing the requirement that $g_I^1 \ll g_{IE}^1$. Linear stability analysis shows that a sufficient condition for the normal visual state to be unstable to spontaneous spatial order is

$$\frac{g_I^1}{g_{EE}^1} > \frac{(1-\varphi)f_E' w_{EE}}{(1-\psi)f_I' w_{II}} \quad \textbf{[4]}$$

(see ref. 23). The right-hand side of the above inequality is typically less than one for reasonable parameters. Because, in the

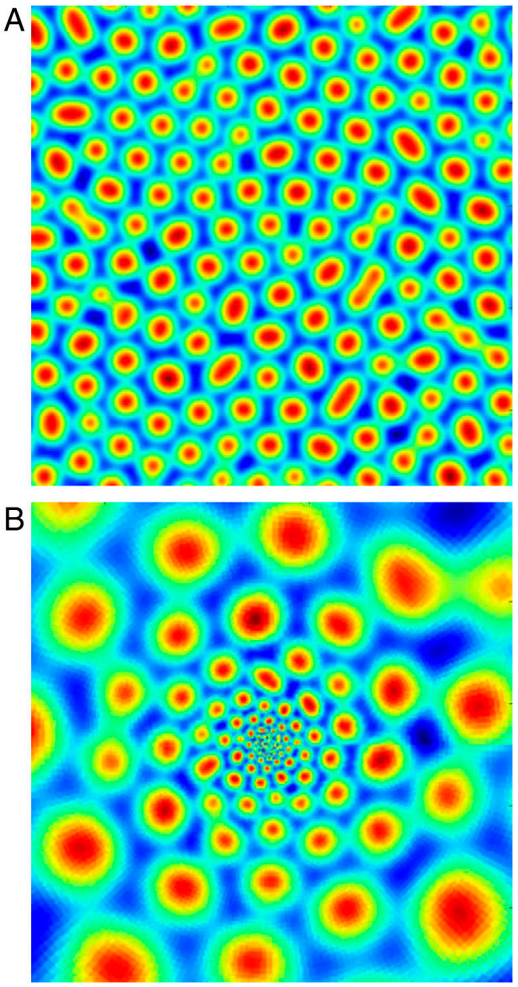

Fig. 2. (*A*) Turing pattern of neural excitation in visual cortex coordinates. (*B*) The same pattern represented in visual field coordinates (i.e., in the coordinates that a patient undergoing geometric visual hallucinations would see). The logarithmic map between visual field and V1 is responsible for the dramatic logarithmic spiral structure of the hallucination. Although the image shown here is from computation, its qualitative features are very similar to those reported by patients (7). Figure generated with the parameters indicated in the text plus $g_{IE}^1 = 6.5$, $g_{II}^1 = 0.1$ with all other $g_{ij}^1 = 1$.

absence of fine tuning, the existence of extensive lattice scale *I–I* connections requires the left-hand side of inequality **4** to be $O(1)$ or greater (to avoid dangling axons between hypercolumns), we can conclude that the requirement that V1 represent visual stimuli through patterns of excitation is incompatible with such *I–I* connections. Only with fine tuning could such *I–I* connections be constructed so as to not generate spontaneous spatial order. Because changing conditions in the brain make such fine tuning impossible, the organization of V1 for robust visual function requires that lattice scale *I–I* connections be sparse. Experimental support for this statement is provided by data on the connections made by a special class of inhibitory cells called large basket cells (LBC), which have long axons and so can provide lattice scale inhibition (14): A recent count (13) of the number of lattice scale inhibitory synapses found on V1 LBC indicates that such connections are sparse compared with the number of lattice scale excitatory synapses found on such neurons and on V1 pyramidal neurons.

The spatial structures that occur in the presence of extensive lattice scale *I–I* coupling differ from those observed in geometric visual hallucinations and contrast with the usual scenario by which a single characteristic length scale emerges from a pattern-forming process. In such a case, the homogeneous steady state is typically unstable for some bounded region of wave vectors greater than zero. Surprisingly, in the case of lattice scale *I–I* connections, the instability occurs for all spatial frequencies greater than some threshold, so that the long wavelength approximation breaks down (see *SI Text*). These effects originate in the suppressive nature of inhibition, captured in the negative sign of the Laplacian for inhibitory connections in Eq. **2**. Laplacian operators with positive signs are associated with signals from excitatory neurons. When the long-range connections are primarily from excitatory neurons, the overall sign of the Laplacian is positive, and the dynamics are those associated with normal diffusion: spatial smoothing if primarily excitatory neurons are excited at long ranges, and Turing patterns if primarily inhibitory neurons are excited at long ranges. When the long-range connections primarily are associated with inhibitory neurons, the overall sign of the Laplacian is negative, leading to reverse diffusion. Reverse, or backward diffusion, has exactly the opposite effect of normal diffusion. Where normal diffusion leads to smoothing of excitations, reverse diffusion leads to clumping of excitations at ever shorter length scales (see Fig. 3). These dynamics rely on the unusual spatial distribution of *I–I* connections. When an inhibitory neuron fires, connected inhibitory neurons at distant lattice sites become less active, allowing excitatory neurons at that site to become more active. Meanwhile, the level of excitation at the original lattice site may be maintained by local feedbacks with excitatory neurons. Close to each of these sites, excitatory activity is suppressed via short range *I–E* or *E–I* connections, unless *E–E* connectivity is strong enough to counteract the overall effect. This local feedback leads to increasingly incoherent local excitations, with activity patterns nearby lattice sites less strongly correlated. If the long-range connections in the network are dominated by *I–I* connections, then increasingly localized clumping of excitations results.

Recent theoretical studies of Turing patterns in reaction-diffusion systems have shown that intrinsic and extrinsic noise enhances the stability of Turing patterns (24–26) through an extension of the quasi-cycle mechanism of McKane and Newman (27, 28). If such results were to hold for pattern formation in V1, achieving robust visual function would be very difficult. We have investigated the effects of noise on the dynamics of our model of V1 and found that, when lattice scale *I–I* connections are sparse, noise does not enlarge the set of parameters that support pat-

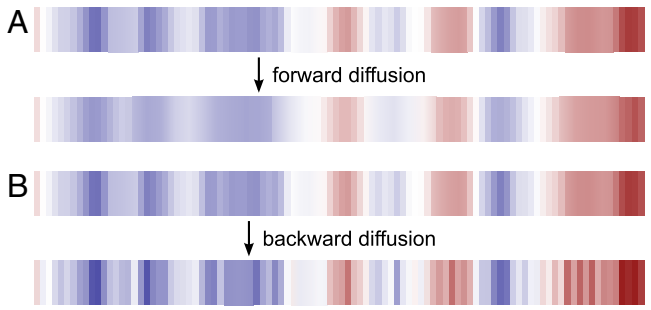

Fig. 3. Schematic representation of how long-range inhibition leads to instability in strips of visual cortex. An excess of excitatory over inhibitory activity is indicated in red and the converse in blue. *A* illustrates dynamics with normal visual cortex architecture, where long-range inhibition is forbidden. These dynamics are analogous to normal diffusion. The upper row shows an initial distribution of activity and the lower row shows the evolution of this distribution at a later time. The spatial distribution of activity is smoothed. *B* illustrates dynamics with added long-range inhibition, whose dynamics are analogous to backward diffusion. The upper row shows the same initial distribution of activity, and the lower row shows the evolution of this distribution at a later time. Under reverse diffusion, the spatial distribution of activity becomes less smooth, leading to short length scale spatial structures.

terns. However, when extensive lattice scale *I–I* coupling is introduced, fluctuation-induced "quasi-patterns" incompatible with normal visual function are generated (see *SI Text*). A further functional role of forbidding such connections may then be avoidance of quasi-pattern generation. We also note that the Turing patterns that do occur in our model of the visual cortex with realistic connectivity are deterministic and highly regular. This behavior is in contrast to most Turing systems, where quasi-patterns dominate and substantial fluctuations in the patterning are expected (24–26). However, it was shown in ref. 29 that Turing patterns generated by noise can be pinned to an underlying lattice provided by the lattice scale patchy *E–E* connections described earlier. The lack of extensive lattice scale inhibitory connections contributes to the stability of such a pinning, and helps to explain, for example, why subjects report seeing geometric visual hallucinations that are highly regular (7).

It should be noted that, although the model we present in Eqs. **1** and **2** is highly simplified, the results are based only on the elementary features of the bifurcation structure of the model. It is well known that the bifurcation structure of models in statistical mechanics and dynamical systems is sensitive to only primitive, detail-independent considerations such as symmetry, fluctuations, range of interaction, and spatial dimension (30, 31). Thus it can be expected that the results will be largely unchanged in more detailed models of V1, which include other standard formulations, such as integrodifferential equations (5) and versions where the lattice structure is explicitly considered.

Discussion

Results on the development of the orientational preference map (9, 21) can be combined with our work to constrain the evolution of several of the basic features of the network anatomy of V1. In refs. 9 and 21, it was shown that, for the orientational preference map of V1 to develop correctly, a lattice scale Mexican hat interaction is required—i.e., short-range amplification and long-range suppression. To achieve this in a two-population excitatory-inhibitory model, either long-range inhibition or long-range *E–I* connections must dominate long-range activation of excitatory neurons. Because our work suggests that extensive lattice scale inhibitory connections are detrimental for normal vision, the only network structure that is consistent with both of these results must have only sparse lattice scale inhibitory connections, and the lattice scale *E–I* connections must have greater effective range than the lattice scale *E–E* connections. However, to avoid hallucinations, the lattice scale *E–I* range must not greatly exceed the local *E–E* range. These V1 circuit properties apply to both the avoidance of hallucinations in normal vision and to the development of orientation preference maps. In fact, both connectivity properties deal with exactly the same problem: breaking the symmetry of translation and orientation preference.

In summary, in V1 the lattice scale network's most elementary features—patchy excitatory connections and sparse inhibitory connections—are completely constrained by two considerations: the need for the visual state to be robust and the developmental requirements of the orientational preference map.

ACKNOWLEDGMENTS. This work was partially supported by National Science Foundation Grant NSF-EF-0526747. Additional funding for T.C.B. was provided through a Drickamer fellowship from the University of Illinois Department of Physics.

1. Hubel DH, Wiesel TN (1974) Uniformity of monkey striate cortex: A parallel relationship between field size, scatter and magnification factor. *J Comp Neurol* 158:295–306.
2. Tootell RBH, Silverman MS, Switkes E, De Valois RL (1982) Deoxyglucose analysis of retinotopic organization in primate striate cortex. *Science* 218:902–904.
3. Passie T, Halpern J, Stichtenoth D, Emrich H, Hintzen A (2008) The pharmacology of lysergic acid diethylamide: A review. *CNS Neurosci Ther* 14:295–314.
4. Turing AM (1952) The chemical basis of morphogenesis. *Philos Trans R Soc B Biol Sci* 237:37–72.
5. Ermentrout GB, Cowan JD (1979) A mathematical theory of visual hallucination patterns. *Biol Cybern* 34:137–150.
6. Bressloff PC, Cowan JD, Golubitsky M, Thomas PJ, Wiener MC (2001) Geometric visual hallucinations, euclidean symmetry and the functional architecture of striate cortex. *Phil Trans R Soc Lond* 356:299–330.
7. Kluver H (1966) *Mescal and Mechanisms of Hallucinations* (Univ Chicago Press, Chicago).
8. Keil W, Schmidt K, Löwel S, Kaschube M (2010) Reorganization of columnar architecture in the growing visual cortex. *Proc Natl Acad Sci USA* 107:12293–12298.
9. Kaschube M, et al. (2010) Universality in the evolution of orientation columns in the visual cortex. *Science* 330:1113–1116.
10. Eldar A, et al. (2002) Robustness of the BMP morphogen gradient in Drosophila embryonic patterning. *Nature* 419:304–308.
11. Gardner T, Cantor C, Collins J (2000) Construction of a genetic toggle switch in Escherichia coli. *Nature* 403:339–342.
12. Tsai T, et al. (2008) Robust, tunable biological oscillations from interlinked positive and negative feedback loops. *Science* 321(5885):126–129.
13. Stepanyants A, Martinez LM, Ferecskó AS, Kisvárday Z (2009) The fractions of short- and long-range connections in the visual cortex. *Proc Natl Acad Sci USA* 106:3555–3560.
14. Markham H, et al. (2004) Interneurons of the neocortical inhibitory system. *Nat Rev Neurosci* 5:793–807.
15. Kisvardy ZF, Beaulieu C, Eysel UT (1993) Network of GABAergic large basket cells in cat visual cortex (area 18): Implication for lateral disinhibition. *J Comp Neurol* 327:398–415.
16. Douglas RJ, Martin KAC (1991) A functional microcircuit for cat visual cortex. *J Physiol* 440:735–769.
17. Bressloff PC, Cowan JD (2002) An amplitude equation approach to contextual effects in visual cortex. *Neural Comput* 14:493–525.
18. Gilbert CD, Wiesel TN (1983) Clustered intrinsic connections in cat visual cortex. *J Neurosci* 3:1116–1133.
19. Bullmore E, Sporns O (2009) Complex brain networks: Graph theoretical analysis of structural and functional systems. *Nat Rev Neurosci* 10:186–198.
20. Watts DJ, Strogatz SH (1998) Collective dynamics of "small-world" networks. *Nature* 393:440–442.
21. Wolf F (2005) Symmetry, multistability, and long-range interactions in brain development. *Phys Rev Lett* 95:208701.
22. Wilson HR, Cowan JD (1972) Excitatory and inhibitory interactions in localized populations of model neurons. *Biophys J* 12:1–22.
23. Ermentrout GB, Cowan JD (1980) Secondary bifurcation in neuronal nets. *SIAM J Appl Math* 323–340.
24. Butler T, Goldenfeld N (2009) Robust ecological pattern formation induced by demographic noise. *Phys Rev E Stat Nonlin Soft Matter Phys* 80:030902.
25. Butler T, Goldenfeld N (2011) Fluctuation-driven Turing patterns. *Phys Rev E Stat Nonlin Soft Matter Phys* 84:011112.
26. Biancalani T, Fanelli D, Di Patti F (2010) Stochastic Turing patterns in the Brusselator model. *Phys Rev E Stat Nonlin Soft Matter Phys* 81:046215.
27. McKane AJ, Newman T (2005) Predator-prey cycles from resonant amplification of demographic stochasticity. *Phys Rev Lett* 94:218102.
28. Wallace E, Benayoun M, van Drongelen W, Cowan JD (2011) Emergent oscillations in networks of stochastic spiking neurons. *PLoS One* 6–e14804.
29. Baker TI, Cowan JD (2009) Spontaneous pattern formation and pinning in the primary visual cortex. *J Physiol Paris* 103:52–68.
30. Cross M, Hohenberg P (1993) Pattern formation outside of equilibrium. *Rev Mod Phys* 65:851–1112.
31. Goldenfeld ND (1992) *Lectures on Phase Transitions and the Renormalisation Group* (Westview, Boulder, CO).

Supporting Information

Butler et al. 10.1073/pnas.1118672109

SI Text

In this supplement, we provide a mathematical treatment of the results reported in the main paper. These results are based upon our analysis of quasi-patterns in the Wilson–Cowan model of the visual cortex. Quasi-patterns are spatial patterns triggered by fluctuations in finite-size networks. Here we show how they can arise in neural networks comprising coupled excitatory and inhibitory populations of simplified model neurons. We then analyze the conditions for such spatial pattern formation, and we show that, depending on the level of long-range inhibition, there are two scenarios. In the first, mean-field effects dominate, and in the second, fluctuation-driven effects.

A Simplified Canonical Microcircuit for Cortical Modules. We first look at modular circuitry. Details of the functional anatomy of a simplified version of the Douglas–Martin canonical microcircuit (1) (our choice for the subblocks of modular circuitry) are shown in Fig. S1). In order to analyze the action of such a circuit, we introduce master equations and actions for neural networks. We first introduce a simple Markov model of the action of a single neuron (2). Each neuron can be in one of two states, quiescent (q) or activated (a). The rate for the transition $q \to a$ is $f[s]$ where f is a smooth saturating function of the input current s, above a current threshold s_{TH}. The rate for the transition $a \to q$ is a constant α.

Following ref. 3, the master equation for $P_{m,n}(t)$, the probability of finding m active excitatory neurons, and n active inhibitory neurons at time t can then be written as

$$\begin{aligned}\frac{dP_{m,n}(t)}{dt} &= \alpha_E[(m+1)P_{m+1,n} - mP_{m,n}] \\ &+ (M-m+1)f_E[s_E(m-1,n)]P_{m-1,n} \\ &- (M-m)f_E[s_E(m,n)]P_{m,n} \\ &+ \alpha_I[(n+1)P_{m,n+1} - nP_{m,n}] \\ &+ (N-n+1)f_I[s_I(m,n-1)]P_{m,n-1} \\ &- (N-n)f_I[s_I(m,n)]P_{m,n}, \end{aligned} \quad \textbf{[S1]}$$

where

$$s_E(m,n) = w_{EE}m - w_{EI}n + h_E, \qquad s_I(m,n) = w_{IE}m - w_{II}n + h_I \quad \textbf{[S2]}$$

are the currents driving the neurons.

Using standard methods (4–7), an equivalent action can be written in the density representation, as

$$\begin{aligned}S = \int dtM\{&(\hat{m}\partial_t m + \hat{p}\partial_t p + \alpha_E m(1-e^{-(\hat{m}-\hat{p})}) \\ &- p(e^{(\hat{m}-\hat{p})}-1)f_E[s_E]) \\ &+ \gamma(\hat{n}\partial_t n + \hat{q}\partial_t q + \alpha_I n(1-e^{-(\hat{n}-\hat{q})}) - q(e^{(\hat{n}-\hat{q})}-1)f_I[s_I])\}, \end{aligned} \quad \textbf{[S3]}$$

where $\gamma = N/M = 0.25$, m and n are densities of active neurons, p and q are densities of quiescent neurons, and $\hat{m}$, $\hat{n}$, $\hat{p}$, and $\hat{q}$ represent the effects of intrinsic fluctuations. Note also that the action $S[m,\hat{m};n,\hat{n};q,\hat{q};p,\hat{p}]$ is that of a single cortical microcircuit, and that $\delta S = \mathscr{L}dt$ where $\mathscr{L}$ is the neural network Lagrangian.

Neocortex as a Two-Dimensional Lattice. We now introduce a model of an extended slice of neocortex as a two-dimensional lattice of canonical microcircuits, however, we first need to distinguish two length-scales. The first we call local, which is the length-scale on which canonical microcircuits interact with their neighbors. We assume that this local scale comprises all the microcircuits in one module. In the simplified model described in this article, we assume that there are nine such microcircuits per module. Thus there are about 1.67×10^4 cells per microcircuit, of which 1.33×10^4 cells are excitatory and 0.33×10^4 cells are inhibitory. Based on neuroanatomical data, we assume that intramodular excitatory and inhibitory connections exist between all microcircuits within a module (8). However, it is also possible, depending on which inhibitory interneurons we choose to model, that the local inhibition is longer ranged than the local excitation.

The second length-scale we call intermediate. On this length-scale, modules are coupled together by patchy excitatory connections. These connections have a range of about ±4 mm with axonal arbors every 1 mm or so (9). Thus they are intermodular. If we take the lattice spacing between individual microcircuits to be L mm, then the intermodular spacing is $\sqrt{a}L$ mm, where a is the number of microcircuits per module. There are also some data on the connections made by a special class of Basket cells called large basket cells, which have long axons and so can provide intermodular inhibition (10). Thus the connections between differing lattice sites support a mixture of both local and intermediate excitation and inhibition, and the currents driving neocortical neurons are now functions of position [i.e., $s_E \to s_i^E(m,n)$, $s_I \to s_i^I(m,n)$] and the intra- and intermodular couplings are as shown in Figs. S2 and S3, respectively.

We can extend both the master equations and the actions derived for a single canonical microcircuit to that of a lattice of such microcircuits simply by indexing them for position in the lattice. Let Ω be the number of microcircuits in the lattice, and let $j = 1,\ldots,\Omega$ denote the lattice coordinates of any microcircuit. Then, for example, the generalization of the action given in Eq. **S3** is

$$\begin{aligned}\int dtM \sum_{j=1}^{\Omega}\{&(\hat{m}_j\partial_t m_j + \hat{p}_j\partial_t p_j + \alpha_E m_j(1-e^{-(\hat{m}_j-\hat{p}_j)}) \\ &- p_j(e^{(\hat{m}_j-\hat{p}_j)}-1)f_E[s_j^E]) \\ &+ \gamma(\hat{n}_j\partial_t n_j + \hat{q}_j\partial_t q_j + \alpha_I n_j(1-e^{-(\hat{n}_j-\hat{q}_j)}) - q_j(e^{(\hat{n}_j-\hat{q}_j)}-1)f_I[s_j^I])\}. \end{aligned} \quad \textbf{[S4]}$$

For a lattice of coupled columns containing microcircuits, the currents given in Eq. **S2** can be written in the form

$$\begin{aligned}s_i^E(m,n) &= g_E(\Delta)w_{EE}m_i - g_I(\Delta)w_{EI}n_i + h_i^E \\ s_i^I(m,n) &= g_E(\Delta)w_{IE}m_i - g_I(\Delta)w_{II}n_i + h_i^I, \end{aligned} \quad \textbf{[S5]}$$

where $g_E(\Delta)$ and $g_I(\Delta)$ are given by

$$\begin{aligned}g_E(\Delta) &= (1+\mu_1^E+\mu_2^E) + \mu_1^E\Delta_1^E + \mu_2^E\Delta_2^E \\ g_I(\Delta) &= (1+\mu_1^I+\mu_2^I) + \mu_1^I\Delta_1^I + \mu_2^I\Delta_2^I \end{aligned} \quad \textbf{[S6]}$$

with

$$\Delta_1^E = \frac{1}{4d}\sum_{j\neq i} - \sum_j \delta_{ij}, \qquad \Delta_2^E = \frac{1}{2d}\sum_{j\neq i} - \sum_j \delta_{ij}. \qquad \textbf{[S7]}$$

Δ_1^E and Δ_2^E are, respectively, the discrete nine- and five-point Laplacian operators in d dimensions, and Δ_1^I, Δ_2^I are defined as the five-point operators

$$\Delta_1^I = \frac{1}{2d}\sum_{j\neq i} - \sum_j \delta_{ij}, \qquad \Delta_2^I = \frac{1}{2d}\sum_{j\neq i} - \sum_j \delta_{ij}. \qquad \textbf{[S8]}$$

The form of Eq. **S6** with terms such as $\mu + \mu\Delta$ is required so that the couplings to neighboring lattice sites can be represented by a Laplacian operator Δ without having on site subtractions (i.e., to cancel the $\sum_j \delta_{ij}$ term in the Laplacian operator). The separate μ_1 and μ_2 terms represent the intra- and interlattice diffusions. In the balance of this supplement, these parameters will be combined.

Writing Eqs. **S6** with the Laplacian operator rather than with explicit indexing allows for simple extraction of continuum equations valid in the long wavelength limit. The continuum representation is convenient for the study of spatial pattern formation carried out in this manuscript.

System-Size Expansion of the Lagrangian. We now carry out the van Kampen system size expansion of the master equation (11). We carry out this expansion on the Lagrangian representation. Alternatively, the master equation can be directly expanded as

$$\mathcal{ME} = \sqrt{M}\mathcal{ME}_1 + \mathcal{ME}_2 + O\left(\frac{1}{\sqrt{M}}\right). \qquad \textbf{[S9]}$$

To carry out the expansion, we assume that the state of the system characterized by (m,n) is at a stable fixed point (φ_0,ψ_0). We then assume that there are Gaussian fluctuations (η,ξ) about this state, so that in general

$$\frac{m}{M} = \varphi + \frac{\eta}{\sqrt{M}}, \qquad \frac{n}{N} = \psi + \frac{\xi}{\sqrt{N}}$$
$$\frac{p}{M} = \vartheta + \frac{\zeta}{\sqrt{M}}, \qquad \frac{q}{N} = \theta + \frac{\xi}{\sqrt{N}}. \qquad \textbf{[S10]}$$

Additionally, the hatted variables are divided by $\sqrt{M}$ and $\sqrt{N}$ as appropriate (see ref. 6 for details of a very similar calculation). Using Eq. **S10** and expanding the exponentials, we obtain the expanded Lagrangian in the form

$$\mathscr{L} = \sqrt{M}\mathscr{L}_1 + \mathscr{L}_2 + O\left(\frac{1}{\sqrt{M}}\right), \qquad \textbf{[S11]}$$

where $M/N = \gamma$ remains constant as we increase both M and N, and

$$\mathscr{L}_1 = \sum_{j=1}^{\Omega}\{[\hat{m}_j\partial_t\varphi_j + \hat{p}_j\partial_t\vartheta_j + \alpha_E\varphi_j(\hat{m}_j - \hat{p}_j) - \vartheta_j(\hat{m}_j - \hat{p}_J)f_E[s_j^E]]$$
$$+ \sqrt{\gamma}[\hat{n}_j\partial_t\psi_j + \hat{q}_j\partial_t\theta_J + \alpha_I\psi_j(\hat{n}_j - \hat{q}_j) - \theta_j(\hat{n}_j - \hat{q}_j)f_I[s_j^I]]\}, \qquad \textbf{[S12]}$$

where

$$s_i^E = g_E(\Delta)w_{EE}\varphi_i - g_I(\Delta)w_{EI}\psi_i + h_i^E$$
$$s_i^I = g_E(\Delta)w_{IE}\varphi_i - g_I(\Delta)w_{II}\psi_i + h_i^I \qquad \textbf{[S13]}$$

and

$$\mathscr{L}_2 = \sum_{j=1}^{\Omega}\left\{\left[\hat{m}_j\partial_t\eta_j + \hat{p}_j\partial_t\zeta_j + \alpha_E\eta_j(\hat{m}_j - \hat{p}_j) - \frac{1}{2}\alpha_E\varphi_j(\hat{m}_j - \hat{p}_j)^2\right.\right.$$
$$\left. - \zeta_j(\hat{m}_j - p_j)f_E[s_j^E] - \frac{1}{2}\vartheta_j(\hat{m}_j - \hat{p}_j)^2 f_E[s_j^E] - \vartheta_j(\hat{m}_j - \hat{p}_j)f'_E\cdot(\delta s_j^E)\right]$$
$$+ \gamma\left[\hat{n}_j\partial_t\xi_j + \hat{q}_j\partial_t\chi_j + \alpha_I\xi_j(\hat{n}_j - \hat{q}_j) - \frac{1}{2}\alpha_I\psi_j(\hat{n}_j - \hat{q}_j)^2\right.$$
$$\left.\left. - \chi_j(\hat{n}_j - q_j)f_E I[s_j^I] - \frac{1}{2}\theta_j(\hat{n}_j - \hat{q}_j)^2 f_I[s_j^I] - \theta_j(\hat{n}_j - \hat{q}_j)f'_I\cdot(\delta s_j^I)\right]\right\}, \qquad \textbf{[S14]}$$

where

$$\delta s_i^E = g_E(\Delta)w_{EE}\eta_i - g_I(\Delta)w_{EI}\xi_i/\sqrt{\gamma}$$
$$\delta s_i^I = g_E(\Delta)w_{IE}\eta_i - g_I(\Delta)w_{II}\xi_i/\sqrt{\gamma}. \qquad \textbf{[S15]}$$

Variational Derivatives of the Lagrangians. If we now form variational derivatives of the Lagrangian, we obtain at $O(\sqrt{M})$

$$\frac{\delta\mathscr{L}_1}{\delta\hat{m}_i} = \partial_t\varphi_i + \alpha_E\varphi_i - \vartheta_i f_E[s_i^E]$$
$$\frac{\delta\mathscr{L}_1}{\delta\hat{p}_i} = \partial_t\vartheta_i - \alpha_E\varphi_i + \vartheta_i f_E[s_i^E]$$
$$\frac{\delta\mathscr{L}_1}{\delta\hat{n}_i} = \sqrt{\gamma}(\partial_t\psi_i + \alpha_I\psi_i - \theta_i f_I[s_i^I])$$
$$\frac{\delta\mathscr{L}_1}{\delta\hat{q}_i} = \sqrt{\gamma}(\partial_t\theta_i - \alpha_I\psi_i + \theta_i f_I[s_i^I]). \qquad \textbf{[S16]}$$

Similarly, at $O(1)$, we obtain

$$\frac{\delta\mathscr{L}_2}{\delta\hat{m}_i} = \partial_t\eta_i + \alpha_E\eta_i - \alpha_E\varphi_i(\hat{m}_i - \hat{p}_i) - \zeta_i f_E[s_i^E]$$
$$- \vartheta_i(\hat{m}_i - \hat{p}_i)f_E - \vartheta_i f'_E\cdot(\delta s_i^E)$$
$$\frac{\delta\mathscr{L}_2}{\delta\hat{p}_i} = \partial_t\zeta_i - \alpha_E\eta_i + \alpha_E\varphi_i(\hat{m}_i - \hat{p}_i) + \zeta_i f_E[s_i^E]$$
$$+ \vartheta_i(\hat{m}_i - \hat{p}_i)f_E + \vartheta_i f'_E\cdot(\delta s_i^E)$$
$$\frac{\delta\mathscr{L}_2}{\delta\hat{n}_i} = \gamma[\partial_t\xi_i + \alpha_I\xi_i - \alpha_I\psi_i(\hat{n}_i - \hat{q}_i) - \chi_i f_I[s_i^I]$$
$$- \theta_i(\hat{n}_i - \hat{q}_i)f_I - \theta_i(f'_I\cdot(\delta s_i^I)]$$
$$\frac{\delta\mathscr{L}_2}{\delta\hat{q}_i} = \gamma[\partial_t\chi_i - \alpha_I\xi_i + \alpha_I\psi_i(\hat{n}_i - \hat{q}_i) + \chi_i f_I[s_i^I]$$
$$+ \theta_i(\hat{n}_i - \hat{q}_i)f_I + \theta_i f'_I\cdot(\delta s_i^I)]. \qquad \textbf{[S17]}$$

Mean-Field Wilson–Cowan Equations. At a minimum, all these variations are zero, whence we obtain at $O(\sqrt{M})$ the equations

$$\partial_t\varphi_i = -\alpha_E\varphi_i + \vartheta_i f_E[s_i^E] \qquad \partial_t\vartheta_i = \alpha_E\varphi_i - \vartheta_i f_E[s_i^E]$$
$$\partial_t\psi_i = -\alpha_I\psi_i + \theta f_I[s_i^I] \qquad \partial_t\theta_i = +\alpha_I\psi_i - \theta f_I[s_i^I]. \qquad \textbf{[S18]}$$

Evidently, we have

$$\partial_t(\varphi_i + \vartheta_i) = 0, \qquad \partial_t(\psi_i + \theta_i) = 0. \qquad \textbf{[S19]}$$

It follows that we can set

$$\varphi_i + \vartheta_i = \text{constant} = 1, \qquad \psi_i + \theta_i = \text{constant} = 1, \qquad \textbf{[S20]}$$

and therefore we can eliminate the equations for the quiescent states p and q, and we are left with the mean-field equations

$$\partial_t \varphi_i = -\alpha_E \varphi_i + (1-\varphi_i) f_E[s_I^E] \qquad \partial_t \psi_i = -\alpha_I \psi_i + (1-\psi_i) f_I[s_I^I]. \tag{S21}$$

With appropriate rescaling, these are the Wilson–Cowan mean-field equations (12), extended to include interactions between patches.

Langevin Equations. In similar fashion, functional derivatives of the $O(1)$ equations yield

$$\begin{aligned}
\partial_t \eta_i &= -\alpha_E \eta_i + \alpha_E \varphi_i (\hat{m}_i - \hat{p}_i) + \zeta_i f_E[s_i^E] \\
&\quad + \vartheta_i (\hat{m}_i - \hat{p}_i) f_E + \vartheta_i f'_E \cdot (\delta s_i^E) \\
\partial_t \zeta_i &= +\alpha_E \eta_i - \alpha_E \varphi_i (\hat{m}_i - \hat{p}_i) - \zeta_i f_E[s_i^E] \\
&\quad - \vartheta_i (\hat{m}_i - \hat{p}_i) f_E - \vartheta_i f'_E \cdot (\delta s_i^E) \\
\partial_t \xi_i &= -\alpha_I \xi_i + \alpha_I \psi_i (\hat{n}_i - \hat{q}_i) + \chi_i f_I[s_i^I] \\
&\quad + \theta_i (\hat{n}_i - \hat{q}_i) f_I + \theta_i f'_I \cdot (\delta s_i^I) \\
\partial_t \chi_i &= \alpha_I \xi_i - \alpha_I \psi_i (\hat{n}_i - \hat{q}_i) - \chi_i f_I[s_i^I] \\
&\quad - \theta_i (\hat{n}_i - \hat{q}_i) f_I - \theta_i f'_I \cdot (\delta s_i^I).
\end{aligned} \tag{S22}$$

Evidently,

$$\partial_t (\eta_i + \zeta_i) = 0, \qquad \partial_t (\xi_i + \chi_i) = 0, \tag{S23}$$

so that we can set

$$\eta_i + \zeta_i = \text{constant} = 0, \qquad \xi_i + \chi_i = \text{constant} = 0 \tag{S24}$$

because all the fluctuations have zero mean.

We can use all these constraints to eliminate the fluctuations ζ and χ, and the noise densities $\hat{p}$ and $\hat{q}$. Let $\hat{u} = \hat{m} - \hat{p}$, $\hat{v} = \hat{n} - \hat{q}$, and let $\zeta = -\eta$, $\chi = -\xi$. Eq. **S22** now reduce to the pair

$$\begin{aligned}
\partial_t \eta_i &= -\alpha_E \eta_i + \alpha_E \varphi_i \hat{u}_i - \eta_i f_E[s_i^E] \\
&\quad + (1-\varphi_i) \hat{u}_i f_E + (1-\varphi_i) f'_E \cdot (\delta s_i^E) \\
\partial_t \xi_i &= -\alpha_I \xi_i + \alpha_I \psi_i \hat{v}_i - \xi_i f_I[s_i^I] \\
&\quad + (1-\psi_i) \hat{v}_i f_I + (1-\psi_i) f'_I \cdot (\delta s_i^I).
\end{aligned} \tag{S25}$$

To obtain fluctuation or Langevin equations, we Fourier transform Eq. **25** with respect to time, and then rewrite the equations of motion for the fluctuations in vector form as

$$i\omega \mathbf{x} = A\mathbf{x} + B\mathbf{y}, \tag{S26}$$

assuming $\mathbf{x}(0) = 0$, and where

$$\mathbf{x} = \begin{pmatrix} \eta \\ \xi \end{pmatrix} \qquad \mathbf{y} = \begin{pmatrix} \hat{u} \\ \hat{v} \end{pmatrix}, \tag{S27}$$

the fluctuation or Langevin equations around homogeneous mean-field steady states φ and ψ, and the matrices A and B are given as

$$A = \begin{pmatrix} -\alpha_E - f_E + & \\ (1-\varphi) f'_E g_E(\Delta) w_{EE} & -(1-\varphi) f'_E g_I(\Delta) w_{EI} / \sqrt{\gamma} \\ (1-\psi) f'_I g_E(\Delta) w_{IE} & -\alpha_I - f_I - (1-\psi) f'_I g_I(\Delta) w_{II} / \sqrt{\gamma} \end{pmatrix} \tag{S28}$$

and

$$BB^\dagger = \begin{pmatrix} \alpha_E \varphi + (1-\varphi) f_E & \cdot \\ \cdot & \alpha_I \psi + (1-\psi) f_I \end{pmatrix}. \tag{S29}$$

These equations describe the dynamics of the fluctuations of the activity η and ξ in terms of the mean-field variables φ and ψ, and the variables $\hat{u}$ and $\hat{v}$. As noted in ref. 13, $\hat{u}$ and $\hat{v}$ are the components of the response field in the Martin–Siggia–Rose response function formalism, and can be therefore considered to be delta-correlated white noise in the direct Langevin equations. The Langevin equations are linear and can therefore be directly solved for moments of the fluctuations. Generalization to fluctuations around more complex mean-field solutions is straightforward, but is not required in the following analysis.

The Emergence of Quasi-Patterns. To calculate the conditions that lead to quasi-patterns, we compute the autocorrelation function $\langle \mathbf{x}_\mathbf{k} \mathbf{x}_\mathbf{k}^\dagger \rangle$ where $\mathbf{x}_\mathbf{k}$ is the Fourier transform of $\mathbf{x}$. The result is that the autocorrelation of the fluctuations of excitatory neurons can be written as

$$\langle \eta_k \eta_k^\star \rangle = \frac{\alpha_k + \beta_k \omega^2}{(\omega^2 - \Omega_k^2)^2 + \Gamma_k^2 \omega^2}, \tag{S30}$$

where

$$\begin{aligned}
\alpha_k &= A_{22}(k)^2 \cdot 2\alpha_E \varphi_0 + A_{12}(k)^2 \cdot 2\alpha_I \psi_0 \\
\beta_k &= 2\alpha_E \varphi_0 \\
\Omega_k^2 &= A_{11}(k) A_{22}(k) - A_{21}(k) A_{12}(k) \\
\Gamma_k &= A_{11}(k) + A_{22}(k),
\end{aligned} \tag{S31}$$

where $\beta_\mathbf{k}$ is obtained from Eq. **S29** evaluated at the fixed point (φ_0, ψ_0), and the $A(k)$ and B coefficients are obtained from Eqs. **S28** and **S29** after a Fourier transformation.

The power spectrum of the fluctuations (for real $\langle \eta_k \eta_k^\star \rangle$) is obtained simply as

$$P_E(k,\omega) = 2 \left\langle \frac{\eta_k}{\sqrt{M}} \frac{\eta_k^\star}{\sqrt{M}} \right\rangle = \frac{2}{M} \frac{\alpha_k + \beta_k \omega^2}{(\omega^2 - \Omega_k^2)^2 + \Gamma_k^2 \omega^2}. \tag{S32}$$

This expression is written in the same format as those in refs. 13 and 14. There is a peak in this spectrum at approximately Ω_k. There is no corresponding peak in the mean-field power spectrum, because there are no fluctuations or oscillations about the mean-field fixed point, which is, in this case, a stable focus.

Mean-Field Conditions for Pattern Formation. The conditions for mean-field spatial pattern formation were worked out initially in ref. 15, and in more detail in ref. 16. The main result is that the lateral inhibition of excitatory cells must be of longer range than that of self-inhibition, and the lateral excitation of inhibitory cells must be of longer range than that of self-excitation. We repeat the analysis within the current formulation, by introducing an additional parameter in the model, the length scale of the intermodular excitation of inhibitory neurons. This additional length scale means that the model must be modified so that instead of a single function $g_E(\Delta)$, we now have two functions, $g_{IE}(\Delta)$ and $g_{EE}(\Delta)$. Additionally, we note that the spatial patterns exist on length scales that exceed the lattice length scale. In the equations of motion, the long relative length scale of the patterns means that the discrete Laplacian can be approximated by its continuum counterpart. Such an approximation is valid.

The form of the currents is then

$$s_i^E = g_{EE}(\Delta)w_{EE}\varphi_i - g_I(\Delta)w_{EI}\psi_i + h_i^E$$
$$s_i^I = g_{IE}(\Delta)w_{IE}\varphi_i - g_I(\Delta)w_{II}\psi_i + h_i^I. \quad \textbf{[S33]}$$

The fields φ and ψ are dimensionless. We rescale the sets of couplings w so that

$$g(\Delta)w = w + g^1 w\Delta, \quad \textbf{[S34]}$$

which defines a set of coupling constants g^1. We assume that when the values of g^1 are varied, the coupling constants w are kept fixed through a rescaling of the original w coupling constants. In the continuum limit, the dimensions of the coupling constants g^1 are L^2. To go to a dimensionless description, we rescale length by $x \to \sqrt{g^1_{EE}}x$ where the new x is a dimensionless length. We also define the ratios $\frac{g^1}{g^1_{EE}} \to g^1$, which puts the currents in the form

$$s_E = w_{EE}(1+\Delta)\varphi - w_{EI}(1+g^1_I\Delta)\psi + h_E$$
$$s_I = w_{IE}(1+g^1_{IE}\Delta)\varphi - w_{II}(1+g^1_I\Delta)\psi + h_I. \quad \textbf{[S35]}$$

In Fourier space, the Laplacian operator $\Delta \to -k^2$, so we expand the coupling matrix $A(\Delta_k) = A(k^2)$ as

$$A(k^2) = A(0) + \frac{dA}{dk^2}k^2 = A_0 + k^2\delta A. \quad \textbf{[S36]}$$

Explicitly, these matrices are

$$A_0 = \begin{pmatrix} -\alpha'_E + (1-\varphi)f'_E w_{EE} & -(1-\varphi)f'_E w_{EI} \\ (1-\psi)f'_I w_{IE} & -\alpha'_I - (1-\psi)f'_I w_{II} \end{pmatrix}, \quad \textbf{[S37]}$$

where we have also rescaled $w_{II}/\sqrt{\gamma} \to w_{II}$ and $w_{EI}/\sqrt{\gamma} \to w_{EI}$ and defined $\alpha' \equiv \alpha + f$. The matrix δA is

$$\delta A = \begin{pmatrix} -(1-\varphi)f'_E w_{EE} & (1-\varphi)f'_E g^1_I w_{EI} \\ -(1-\psi)f'_I g^1_{IE} w_{IE} & (1-\psi)f'_I g^1_I w_{II} \end{pmatrix}. \quad \textbf{[S38]}$$

Note that the matrix B is unaffected by these rescalings.

To obtain the conditions for mean-field pattern formation, we must obtain the eigenvalues of $A(k)$. Mean-field pattern formation occurs when the eigenvalues of $A(0)$ are negative, but for some finite range of $k \neq 0$, the eigenvalues become nonnegative (17). The eigenvalues are given by the equation

$$\lambda_\pm = \frac{1}{2}\left[\mathrm{Tr}A \pm \sqrt{(\mathrm{Tr}A)^2 - 4\det A}\right]. \quad \textbf{[S39]}$$

But $\lambda_+ \geq \lambda_-$, so we need only investigate λ_+ to find the transition to pattern formation.

It is clear from the eigenvalue formula that a necessary condition for spatial pattern formation is $\det A \leq 0$, for then $\lambda_+ \geq 0$. From Eq. **S34**, we can expand $\det A$ as

$$\det A = \det A_0 + \Delta A k^2 + \det \delta A k^4, \quad \textbf{[S40]}$$

where $\Delta A = \delta A_{11}A_{22} + A_{11}\delta A_{22} - \delta A_{12}A_{21} - A_{12}\delta A_{21}$.

It follows that we can obtain the necessary condition for spatial pattern formation, $\det A \leq 0$ over a finite range of wave numbers k if and only if

$$\Delta A < 0, \qquad \det \delta A > 0 \qquad 4\det A_0 \det \delta A < (\Delta A)^2. \quad \textbf{[S41]}$$

These conditions are obtained from seeking zeros of the biquadratic Eq. **S40** in k.

Pattern Formation Beyond Mean Field. To calculate the conditions under which patterns form beyond mean field, we follow ref. 6. We assume that mean-field solutions are stable and constant. We set $\omega = 0$ and examine the power spectrum in the form

$$P_E(k,0) = \frac{2}{M}\frac{A_{22}(k)^2(2\alpha_E\varphi_0) + A_{12}(k)^2(2\alpha_I\psi_0)}{|\det(A(k))|^2}, \quad \textbf{[S42]}$$

where $A(k,0)$ is strictly real.

To obtain the conditions for pattern formation, we note that the denominator of this equation will grow as the eighth power of k in the large k limit, so the power spectrum will be a decreasing function of k for large k. Thus a sufficient condition for pattern formation (corresponding to a nonzero peak in the power spectrum) is that $dP_E/dk^2 > 0$. To evaluate the conditions under which this inequality is satisfied, we examine the derivative

$$\frac{d}{dx}\frac{f}{g^2} = \frac{f'g - 2fg'}{g^3}. \quad \textbf{[S43]}$$

Dropping constant factors and taking $f = A_{22}(k)^2B_1^2 + A_{12}(k)^2B_2^2$ and $g = \det[A(k)]$ (to satisfy the sufficient condition for pattern formation), we find the condition for fluctuation-driven pattern formation in excitatory neurons to be

$$(A^0_{22}\delta A_{22}B_1^2 + A^0_{12}\delta A_{12}B_2^2)\det(A^0) > (A^0_{22}{}^2B_1^2 + A^0_{12}{}^2B_2^2)\Delta A. \quad \textbf{[S44]}$$

We also want the criteria for fluctuation-driven pattern formation in the inhibitory neuron population. To obtain this criteria, we note that the power spectrum for inhibitory fluctuations is

$$P_I(k,0) = \frac{2}{M}\frac{A_{21}(k)^2(2\alpha_E\varphi_0) + A_{11}(k)^2(2\alpha_I\psi_0)}{|\det(A(k))|^2}. \quad \textbf{[S45]}$$

Through simple substitution of the explicit subscripts $22 \to 21$ and $12 \to 11$ we obtain the conditions for pattern formation in the inhibitory neurons as

$$(A^0_{21}\delta A_{21}B_1^2 + A^0_{11}\delta A_{11}B_2^2)\det A_0 > (A^0_{21}{}^2B_1^2 + A^0_{11}{}^2B_2^2)\Delta A. \quad \textbf{[S46]}$$

This condition differs slightly from that for excitatory neurons.

For completeness, we next obtain the conditions for quasi-cycles by setting $k = 0$ and retaining ω^2. Through identical calculations to those above with the independent variable k^2 replaced by ω^2, the condition for quasi-cycles is obtained

$$\beta_k \det A_0 > \alpha_k(\mathrm{Tr}^2A_0 - 2\det A_0) \quad \textbf{[S47]}$$

with $\beta_k > 0$ and $\alpha_k > 0$ as defined in Eq. **S31** (with $k^2 = 0$).

Pattern Formation with Inhibition Forbidden in the Intermediate Length Scale. The most important case anatomically is the case where there are no inhibitory synapses at the intermediate length scale. In this case, the parameters satisfy $g^1_{EE} \gg g^1_I$ and $g^1_{IE} \gg g^1_I$. Under these conditions, the left-hand side of Eq. **S44** is order g^1_I, and so its magnitude is much less than the right-hand side, which is of higher order. So, to achieve fluctuation-driven pattern formation, to order g^1_I the requirement is $\Delta A < 0$.

From the explicit form of the explicit determinant of δA,

$$\det \delta A = (1-\varphi)(1-\psi)f'_I f'_E g^1_I[g^1_{IE}w_{EI}w_{IE} - g^1_{EE}w_{EE}w_{II}], \quad \textbf{[S48]}$$

the left-hand side of the last equation of the mean-field pattern formation conditions Eq. **S41** is $[O(g_I^1)]$. ΔA is not generally small. This condition implies that in the case of no intermediate inhibitory connections, the requirement for mean-field pattern formation is $O(g_I^1) < \Delta A^2$, Thus, in this case, the conditions for fluctuation-driven and mean-field pattern formation are identical to order g_I^1, provided $\det \delta A > 0$.

To derive the condition explicitly, terms in Eq. **S44** of order g_I^1 can be neglected, whence

$$\Delta A = g_{IE}^1(1-\psi)f_I' w_{IE} A_{12} - g_{EE}^1(1-\varphi)f_E' w_{EE} A_{22} < 0. \quad \textbf{[S49]}$$

Rearranging yields

$$\frac{g_{IE}^1}{g_{EE}^1} > \frac{w_{EE}[\alpha_I' + (1-\psi)f_I' w_{II}]}{w_{EI}(1-\psi)f_I' w_{IE}} + O\left(\frac{g_I^1}{g_{EE}^1}\right). \quad \textbf{[S50]}$$

This equation describes the conditions under which patterns can form, provided there are no intermediate length-scale inhibitory-inhibitory connections.

Short Length-Scale Spatial Effects. In addition to spatial pattern formation, the stability matrix A yields eigenvalues that increase without bound as a function of k until the continuum approximation breaks down somewhere near the length scale of the lattice spacing. This instability corresponds to short length-scale spatial structure. This possibility arises because there are several ways that the eigenvalue can become positive for nonzero k. The first way is for $\mathrm{Tr}A$ to become positive. In the standard formulation of Turing instabilities, this is forbidden, but in the model currently being investigated, this is a possibility. The key physical difference is that, in the standard Turing models, diffusion of inhibitor into a neighboring cell increases the local concentration of inhibitor. This normal diffusive behavior does not take place in neural inhibition, which reduces the amount of activity in neighboring inhibitors, and which is opposite the effect of normal diffusion, resulting in time-reversed diffusion dynamics as discussed in the main text.

The formula for $\mathrm{Tr}A(k)$ is

$$\mathrm{Tr}A = \mathrm{Tr}A_0 + [(1-\psi)f_I' g_I^1 w_{II} - (1-\varphi)f_E' w_{EE}]k^2. \quad \textbf{[S51]}$$

Thus, if

$$\frac{g_I^1}{g_{EE}^1} > \frac{(1-\varphi)f_E' w_{EE}}{(1-\psi)f_I' w_{II}}, \quad \textbf{[S52]}$$

λ_+ increases without bound as a function of increasing k (note we have restored g_{EE}^1 for clarity). An additional condition for unbounded growth of λ_+ is can be obtained by noting that, if

$$\det \delta A < 0, \quad \textbf{[S53]}$$

then the eigenvalue will increase as k^2 as well.

A plot of eigenvalues of A in both the mean-field pattern-forming phase and the short length-scale spatially structured phase is shown in Fig. S4.

Because of the long wavelength approximations contained in the above calculations, characterizing the short length-scale spatially structured phase requires simulation at the lattice scale. A representative simulation in this phase is shown in Fig. S5.

Phase Diagram when Inhibition is Introduced at the Intermediate Length Scale. As noted above, in the visual cortex (and in the neocortex more generally) inhibition over the intermediate length scale is forbidden. Anatomical studies cannot explain why the neural architecture is configured in this way. However, the current model can be modified to see how its qualitative behavior would differ if intermediate length-scale inhibition were introduced. Whereas the model is a highly simplified caricature of the real neocortex, the qualitative features that emerge when intermediate inhibition is introduced are likely to illuminate the real changes in function that would occur in the brain if such couplings existed. In this section, we report the behavior of the system as a function of the longest length scale of inhibitory and excitatory connections.

When intermediate length-scale inhibition is introduced, the neocortex is overwhelmed by spontaneous spatiotemporal dynamics. Analytically, this spontaneous activity can be seen in Eq. **S52**, which shows that, if g_I^1 is sufficiently large, the system spontaneously generates spatial structure. If intermediate length-scale inhibition is forbidden, the model has rich phase behavior, including short length scale structure generated by backward diffusion, homogeneous steady states, and pattern formation. In the visual cortex in particular, there must be a stable homogeneous phase so that sensory data can determine the excitation patterns of the neurons rather than internally generated activity.

To study these behaviors systematically, we explored the above conditions numerically. The result is that increasing the length scale of inhibition increases substantially the likelihood that intrinsic fluctuations will trigger the formation of spatial structures. Fig. S6 shows the phase diagram.

Summary. In this supplement, we have shown how intrinsic fluctuations in networks of excitatory and inhibitory neurons completely change their dynamics. In particular, we have shown that, in case their mean-field dynamics is at a stable focus, then the fluctuations about such a focus trigger persistent noisy oscillations or quasi-cycles, and/or the emergence of spatial activity patterns or quasi-patterns in case the fixed point is also spatially homogeneous.

1. Douglas RJ, Martin KAC (1991) A functional microcircuit for cat visual cortex. *J Physiol* 440:735–769.
2. Cowan JD (1990) Stochastic neurodynamics. *Adv Neural Inf Process Syst* 3:62–69.
3. Benayoun M, Cowan J, Van Drongelen W, Wallace E (2010) Avalanches in a stochastic model of spiking neurons. *PLoS Comp Biol* 6:e1000846.
4. Doi M (1976) Second quantization representation for classical many particle system. *J Phys A Math Gen* 9:1465–1479.
5. Peliti L (1985) Path integral approach to birth death processes on a lattice. *J Phys* 46:1469–1483
6. Butler T, Goldenfeld N (2009) Robust ecological pattern formation induced by demographic noise, *Phys Rev E Stat Nonlin Soft Matter Phys* 80:030902.
7. Goldenfeld N (1984) Kinetics of a model for nucleation-controlled polymer crystal growth. *J Phys A Math Gen* 17:2807–2821.
8. Bressloff PC, Cowan JD (2002) An amplitude equation approach to contextual effects in visual cortex. *Neural Comput* 14:493–525.
9. Gilbert CD, Wiesel TN (1983) Clustered intrinsic connections in cat visual cortex. *J Neurosci* 3:1116–1133.
10. Markham H, et al. (2004) Interneurons of the neocortical inhibitory system *Nat Rev Neurosci* 5:793–807.
11. van Kampen NG (1992) *Stochastic Processes in Physics and Chemistry* (Elsevier, New York).
12. Wilson HR, Cowan JD (1972) Excitatory and inhibitory interactions in localized populations of model neurons. *Biophys J* 12:1–22.
13. Butler T, Reynolds D (2009) Predator-prey quasicycles from a path integral formalism. *Phys Rev E Stat Nonlin Soft Matter Phys* 79:032901.
14. Lugo C, McKane AJ (2008) Quasicycles in a spatial predator-prey model. *Phys Rev E Stat Nonlin Soft Matter Phys* 78:051911.
15. Wilson HR, Cowan JD (1973) A mathematical theory of the functional dynamics of cortical and thalamic nervous tissue. *Kybernetik* 13:55–80.
16. Ermentrout GB, Cowan JD (1980) Large scale spatially organized activity in neural nets. *SIAM J Appl Math* 38:1–21.
17. Turing AM (1953) The chemical basis of morphogenesis, *Philos Trans R Soc Lond B Biol Sci* 237:37–72.

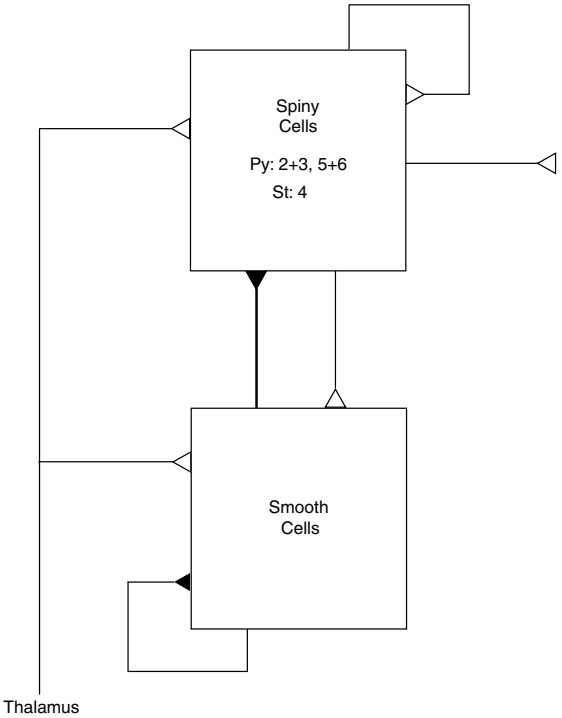

Fig. S1. Block diagram of a reduced neocortical microcircuit. Py, pyramidal neurons; St, spiny stellate neurons; unfilled triangles, excitatory synapses; filled triangles, inhibitory synapses.

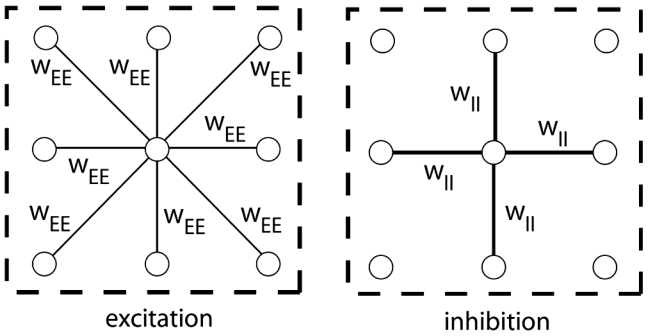

Fig. S2. Block diagram of intramodular coupling.

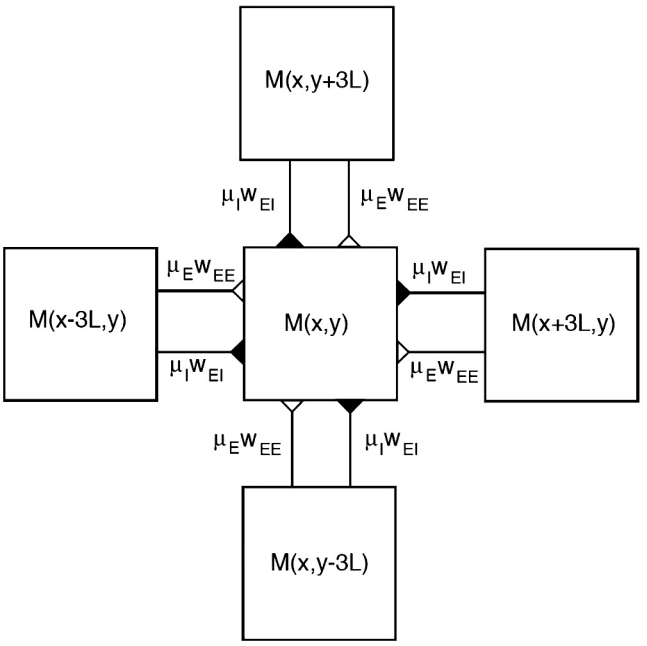

Fig. S3. Block diagram of intermodular coupling.

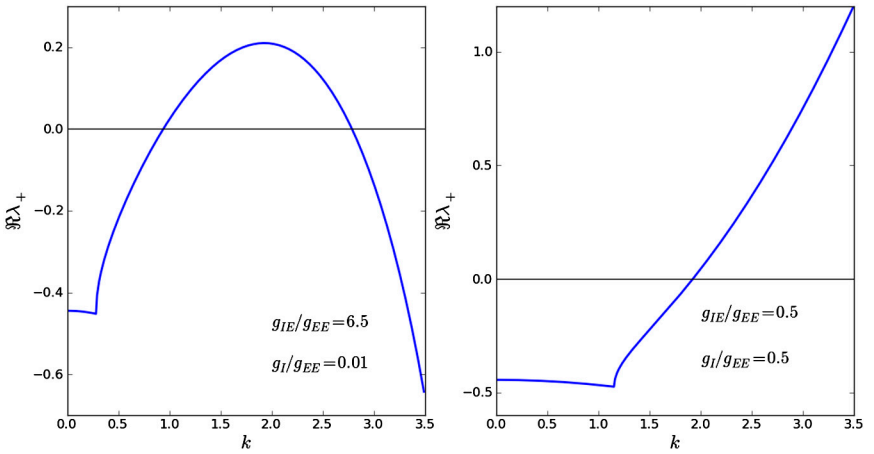

Fig. S4. The real part of the largest eigenvalue of the stability matrix as a function of k for the case of spatial pattern formation (*Left*) and for the case of unbounded growth (*Right*).

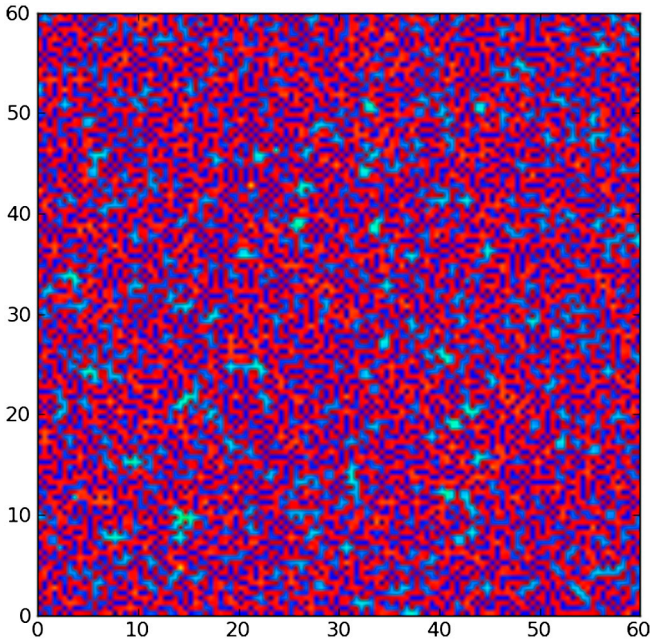

Fig. S5. Simulation of lattice neural dynamics in the short length-scale spatially structured phase. The results show that in the short length-scale spatially structured phase, the spatial structure is sharp on the lattice scale and distinct from regular pattern formation.

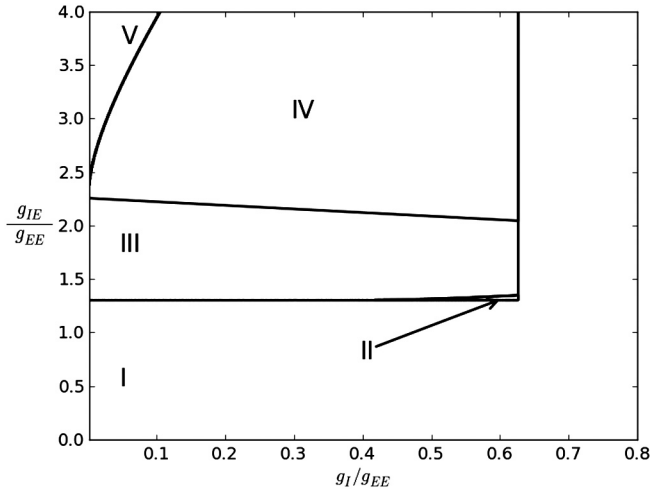

Fig. S6. Phase diagram for pattern formation. This figure shows the conditions for the emergence of spatial structure. Region I is short length-scale spatial structure at the mean-field level, region II is a mean-field pattern formation phase, region III is a homogeneous steady state phase, region IV is the quasi-pattern phase, and region V is a mean-field pattern-forming phase.